IEEE Access
Multidisciplinary | Rapid Review | Open Access Journal

Received January 18, 2019, accepted February 12, 2019, date of publication February 18, 2019, date of current version March 8, 2019.

Digital Object Identifier 10.1109/ACCESS.2019.2899991

Response Diversity of Stub-Loaded Ring Bandpass Filter Based on Commensurate Line Element: Single- and Dual-Band Applications

XIUHUA JIN, XIAODONG HUANG, (Member, IEEE), DONG CHEN, AND CHONGHU CHENG, (Member, IEEE)

College of Telecommunications and Information Engineering, Nanjing University of Posts and Telecommunications, Nanjing 210003, China

Corresponding author: Xiaodong Huang (xdhuang@njupt.edu.cn)

This work was supported in part by the NUPTSF under Grant NY214141, and in part by the National Natural Science Foundation of China under Grant 61501257, Grant 61501258, Grant 61427801, and Grant U1636108.

ABSTRACT Response diversity of a commensurate line bandpass filter is described and discussed. It is found that a stub-loaded ring topology can generate different bandpass responses in a single band or two symmetric bands, depending on the line admittances in the topology. For a single band, the response can be designed to be an equiripple delay, Chebyshev in magnitude, or elliptic in magnitude. For dual bands, the out-band attenuation curve can be adjusted with almost unchanged in-band matching. A generalized synthesis algorithm, supporting both the single- and dual- band applications, is given to calculate the admittance of each line element, according to the prescribed in-band specifications, e.g., ripple factor and cut-off frequencies. Further study reveals that the admittance of the line segment between the stubs is the key element dominating the response type in the single-band case. When the admittance is positive, zero, and negative, the response is an equiripple delay, Chebyshev in magnitude, and elliptic in magnitude, respectively. To validate the synthesis algorithm, four filter sets with different responses are given and simulated through a transmission line model. For circuit verification, a microstrip filter with a single-band elliptic response is designed, fabricated, and measured, of which the negative admittance line is realized by a coupled line section with shorted ends. The experimental results show that the filter achieves elliptic response successfully. The measured 3-dB fractional bandwidth is 86.6% centered at 0.97 GHz, within which the minimal insertion loss is 0.88 dB at 0.81 GHz. Furthermore, two transmission zeroes beside the passband are observed clearly at 0.31 and 1.59 GHz, offering a sharp rejection in the stopband.

INDEX TERMS Bandpass filter, wideband filter, filter synthesis, transmission zero, dual-band.

I. INTRODUCTION

Wideband bandpass filter (BPF) became extremely attractive after the releasing of Ultra-Wideband spectrum in 2002 by the Federal Communications Commission [1]. In order to cover such a wide frequency band from 3.1 to 10.6 GHz, the fractional bandwidth (FBW) should exceed over 100%, which is hardly met using the classic filter synthesis theory developed based on narrow band approximations [2], [3]. Therefore, this urgent demand leads to many new design theories for wideband BPF [4], such as the multiple mode resonance (MMR) [5]–[9], stub-loaded topology [8]–[13], and the signal interference technology [14]–[17].

The MMR was firstly reported by Zhu et al. [5] in 2005, and soon became the most focused concept in wideband filter design area. By using two or more resonant modes simultaneously in a finely tuned individual resonator, a continuous and flat frequency response over 100% FBW can be built with a proper feeding scheme [5]. The related researches on the MMR-based BPF include band-notch [6], harmonic suppression [7], mathematical synthesis [8], [9], and so on. The stub-loaded topology is a classic structure which supports

The associate editor coordinating the review of this manuscript and approving it for publication was Roberto Gomez-Garcia.

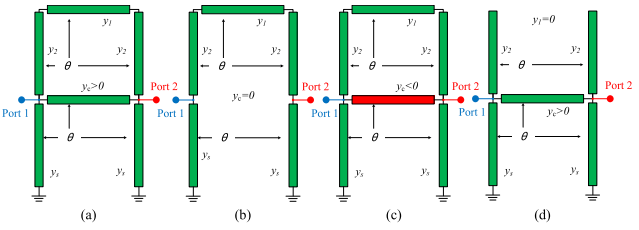

FIGURE 1. Configurations of stub loaded ring filter. (a) Bottom line with positive admittance, the common case. (b) Bottom line with zero admittance. (c) Bottom line with negative admittance. (d) Top line with zero admittance.

wideband filter applications, in which several short/open ended stubs are arranged in sequence and separated by transmission line segments [8]–[13]. When all the stubs and line segments are equal in electrical length, namely commensurate, this topology enables the facilitation in mathematical modeling and analysis, but, suffers from relatively large size due to its cascading structure [11]–[13]. Besides, the circuit area can be reduced by folding the connecting line into a coupled line section, with an improved equiripple delay response [14]. The signal interference is another new concept in filter design [15]–[18]. The reduction in circuit area and the steep rejection in stopband can be achieved simultaneously, by introducing one or more interferences from the multiple signal passages between the input/output ports [15]. The main drawback of this technique is the lack of precise synthesis methods [16], [17], especially for equiripple response. In most of the reported wideband BPF designs, the group delay characteristic is ignored or fixed, because the design methodologies are derived entirely from magnitude response. In our recent works, two new wideband BPFs are given to show the co-existence of equiripple responses in both delay and magnitude, one of which is utilized by coupled lines section [14] while the other one is achieved by commensurate line ring [18]. The common part of the two BPFs in structure is a pair of short-ended stubs.

In this work, we will give a full demonstration on the responses based on the filter topology reported originally in [18], in the consideration of the passband number, delay, transmission zero, and circuit realization. The objective of this study is to reveal the response diversity/complexity of the stub-loaded ring structure, and the unity/simplicity in mathematical representation. It will be shown that four filters of different types [9], [12], [13], [15], [16], [18] and different operation mechanisms have a common prototype in topology and can be analyzed through a generalized algorithm. Besides, all of the following discussions are based on equiripple magnitude response in passband, which is guaranteed by using an improved synthesis approach based on [18].

II. FILTER TOPOLOGY, SYNTHESIS AND REALIZATION

Fig.1 shows the configurations of the stub loaded ring filters. As given in Fig.1a, the initial filter is composed of six line components, with normalized admittances of y_1, y_2, y_c, y_2, y_s, and y_s, respectively. Four of them (y_1, y_2, y_c, and y_2) form a closed ring, and the other two (y_s and y_s) are used as short-ended stubs loaded beside the bottom section (y_c) of the ring. All of the line segments have an identical electrical length (θ).

According to [18], the overall transfer function F_{cir} can be expressed by the admittances (y_i) of the filter, as follows,

$$F_{cir}(x^2) = j\frac{a_0 + a_2x^2 + a_4x^4 + a_6x^6 + x^8}{b_0 + b_2x^2 + b_4x^4 + b_6x^6} \qquad x \in (-\infty, +\infty) \tag{1}$$

in which

$$\begin{cases} \boldsymbol{a_0} = \dfrac{-y_1^2 + y_2^4 - 2y_1y_2^2y_c + y_1^2y_c^2}{16y_2y_s\left(2y_1y_2 + 4y_1y_c + 2y_2y_c + 2y_1y_s + y_2y_s\right)} \\ \boldsymbol{a_2} = \dfrac{\begin{array}{c}(2y_1y_2 + y_2{}^2 - y_1{}^2y_2{}^2 - 2y_1y_2{}^3 - 2y_1{}^2y_2y_c + \\ -6y_1y_2{}^2y_c - 2y_2{}^3y_c - 2y_1y_2y_c{}^2 - y_2{}^2y_c{}^2 - 2y_1{}^2y_2y_s + \\ -2y_1y_2{}^2y_s - 2y_2{}^3y_s - 2y_1{}^2y_cy_s - y_1{}^2y_s{}^2)\end{array}}{4y_2y_s\left(2y_1y_2 + 4y_1y_c + 2y_2y_c + 2y_1y_s + y_2y_s\right)} \\ \boldsymbol{b_0} = \dfrac{y_1\left(y_2{}^2 - y_1y_c\right)}{8y_2y_s\left(2y_1y_2 + 4y_1y_c + 2y_2y_c + 2y_1y_s + y_2y_s\right)} \\ \boldsymbol{b_6} = \dfrac{y_1y_2{}^2 + 2y_1y_2y_c + y_2{}^2y_c}{y_2y_s\left(2y_1y_2 + 4y_1y_c + 2y_2y_c + 2y_1y_s + y_2y_s\right)} \\ a_4 = 1 + \boldsymbol{a_2} \\ a_6 = 2 \\ b_2 = 2\boldsymbol{b_0} + \dfrac{\boldsymbol{b_6}}{2} \\ b_4 = \dfrac{3\boldsymbol{b_6}}{2} \end{cases} \tag{2}$$

and

$$\frac{x}{\sqrt{1+x^2}} = \frac{tan\,(\theta/2) - 1}{tan\,(\theta/2) + 1} \qquad \theta \in \left[0, 180^\circ\right] \tag{3}$$

The variable transformation ($x \leftrightarrow \theta$) in (3) extends the initial definition domain (θ) of $F_{\rm cir}$ to the field of real number (x), for the ease of polynomial synthesis. If any passband and in-band ripple exist, even number of solutions must be found on the real axis for $F_{\rm cir} = 0$, then one or two passbands across the solutions (zeroes) can be defined by a ripple factor (ε), as well as the cut-off frequencies.

As shown in Fig.2, a real rational function $F_{\rm ideal}$, having the same structure of $-jF_{\rm cir}$ of (1), is implemented and drawn with four zeroes and three extrema at $-x_{\rm m}(\theta_{\rm m})$, $0(\theta = 90^\circ)$, and $x_{\rm m}(\theta_{\rm m}')$. Let $\varepsilon = |F_{\rm ideal}(x_{\rm m})|$, then two discrete passbands can be determined from $-x_{\rm c1}$ to $-x_{\rm c2}$, and $x_{\rm c2}$ to $x_{\rm c1}$, respectively. Particularly, the two passbands will be merged into a continuous single passband when $x_{\rm c2} = 0$ ($\theta_{\rm c2} = 90^\circ$), yields the same curve and solutions as those in [18].

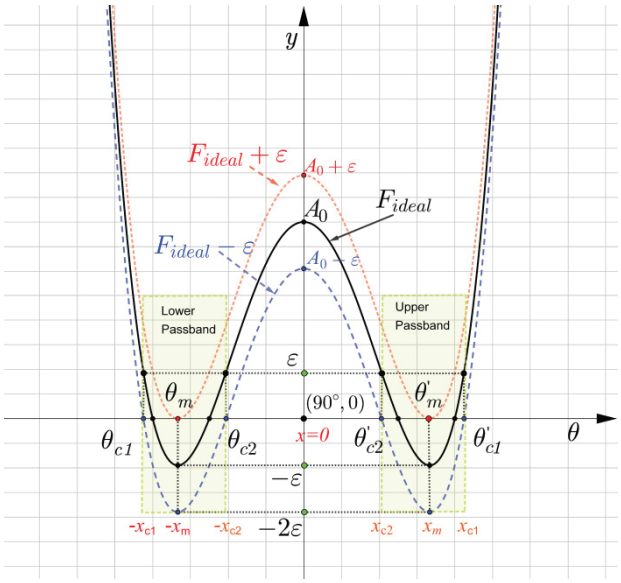

FIGURE 2. Transfer function with equiripple response in magnitude (centered at $\theta = 90°$).

Therefore, by defining three in-band specifications (ε, θ_{c1} and θ_{c2}) and an extra variable θ_m, satisfying

$$\begin{cases} FBW^D = \dfrac{2(\theta_{c2}-\theta_{c1})}{(\theta_{c2}+\theta_{c1})}, \\ \qquad for\ the\ 1st\ passband\ of\ dual-band \\ FBW^S = 2\left(1-\dfrac{\theta_{c1}}{90°}\right), \\ \qquad for\ single-band\ (\theta_{c2}=90°) \\ \varepsilon \quad = 10^{S/20}\left(1-10^{S/10}\right)^{-0.5}, \quad S\ is\ the\ Ripple\ of \\ \qquad |S_{11}|\ in\ dB \\ \theta_m\ is\ the\ location\ of\ the\ 1st\ Ripple\ in\ the\ 1st\ passband \end{cases} \tag{4}$$

the goal transfer function of prescribed in-band properties can be established. In [18], we have proposed a full synthesis procedure of F_{ideal} on the single-band case. Here, an updated approach is presented with the supporting of dual-band response. As mentioned above, F_{ideal} should have the same structure of -jF_{cir}, that is

$$\begin{aligned} F_{ideal}\left(x^2\right) &= \frac{c_0+c_2x^2+c_4x^4+c_6x^6+x^8}{d_0+d_2x^2+d_4x^4+d_6x^6} \\ &= \varepsilon\frac{P\left(x^2\right)}{Q\left(x^2\right)} = \varepsilon f\left(x^2\right) \end{aligned} \tag{5}$$

where

ε is a positive number, represents the ripple factor in magnitude

c_i and $d_i (i = 0, 2, 4, 6)$ are real numbers

$f(x^2)$ is the normalized form of $F_{ideal}(x^2)$ with ripple factor of 1

For calculating the coefficients of (5), other two functions are given here based on $f(x^2)$, as

$$\begin{aligned} f^{\pm1}\left(x^2\right) &= f\left(x^2\right)\pm 1 = \frac{P\left(x^2\right)\pm Q\left(x^2\right)}{Q\left(x^2\right)} \\ &= \frac{c_0^{\pm}x^0+c_2^{\pm}x^2+c_4^{\pm}x^4+c_6^{\pm}x^6+x^8}{Q\left(x^2\right)} \end{aligned} \tag{6}$$

From Fig.2, it is obvious that $f^{\pm1}\left(x^2\right)$ have the following forms due to the distributions of roots and ripples.

$$\begin{cases} f^{+1}\left(x^2\right) = \dfrac{\left(x^2-x_m^2\right)^2\left(x^4+K_1x^2+K_2\right)}{Q\left(x^2\right)} \\ f^{-1}\left(x^2\right) = \dfrac{\left(x^2-x_{c1}^2\right)\left(x^2-x_{c2}^2\right)\left(x^4+K_3x^2+K_4\right)}{Q\left(x^2\right)} \end{cases} \tag{7}$$

where

$$\begin{cases} x^4+K_1x^2+K_2>0 \\ x^4+K_3x^2+K_4>0 \end{cases} \tag{8}$$

Hence, the coefficients of $f^{\pm1}(x^2)$ can be expressed as

$$\begin{cases} c_0^+ = K_2x_m^4 \\ c_2^+ = -2K_2x_m^2+K_1x_m^4 \\ c_4^+ = K_2+x_m^4-2K_1x_m^2 \\ c_6^+ = K_1-2x_m^2 \\ c_0^- = 0 \\ c_2^- = -2K_4\left(x_{c1}^2+x_{c2}^2\right)+K_3x_{c1}^2x_{c2}^2 \\ c_4^- = K_4-K_3\left(x_{c1}^2+x_{c2}^2\right)+x_{c1}^2x_{c2}^2 \\ c_6^- = K_3-\left(x_{c1}^2+x_{c2}^2\right) \end{cases} \tag{9}$$

Then, the coefficients of $F_{\text{ideal}}(x^2)$ can be obtained

$$\begin{cases} c_i = \dfrac{\left(c_i^+ + c_i^-\right)}{2} \\ d_i = \dfrac{\left(c_i^+ - c_i^-\right)}{2\varepsilon} \end{cases} \qquad i = 0,\ 2,\ 4,\ 6 \tag{10}$$

That is

$$\begin{cases} c_0 = \dfrac{K_4x_{c1}^2x_{c2}^2+K_2x_m^4}{2} \\ c_2 = \dfrac{-2K_2x_m^2-K_4\left(x_{c1}^2+x_{c2}^2\right)+K_1x_m^4+K_3x_{c1}^2x_{c2}^2}{2} \\ c_4 = \dfrac{K_2+K_4-2K_1x_m^2-K_3\left(x_{c1}^2+x_{c2}^2\right)+x_m^4+x_{c1}^2x_{c2}^2}{2} \\ c_6 = \dfrac{K_1+K_3-2x_m^2-\left(x_{c1}^2+x_{c2}^2\right)}{2} \\ d_0 = \dfrac{-K_4x_{c1}^2x_{c2}^2+K_2x_m^4}{2\varepsilon} \\ d_2 = \dfrac{K_1x_m^4-2K_2x_m^2+K_4x_c^2}{2\varepsilon} \\ d_4 = \dfrac{K_2-2K_1x_m^2+x_m^4-K_4+K_3x_c^2}{2\varepsilon} \\ d_6 = \dfrac{K_1-2x_m^2-K_3+x_c^2}{2\varepsilon} \end{cases} \tag{11}$$

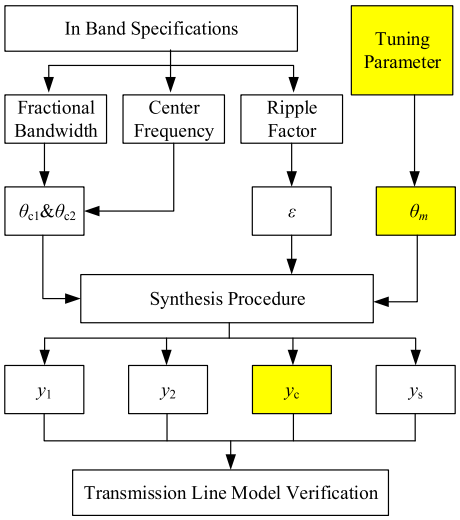

FIGURE 3. Design procedure of stub loaded ring filter.

Because $F_{\text{ideal}}(x^2)$ is the goal response of F_{cir}, their coefficients must have the same relationships in (2), namely,

$$\begin{cases} c_4 = 1 + c_2 \\ c_6 = 2 \\ d_2 = 2d_0 + d_6/2 \\ d_4 = 3d_6/2 \end{cases} \tag{12}$$

Solve (11) with (12), we have

$$\begin{cases} K_1 = 2 + x_{c1}^2 + x_{c2}^2 \\ K_2 = 1 + x_{c1}^2 + x_{c2}^2 + x_{c1}^2 x_{c2}^2 \\ K_3 = 2\left(1 + x_m^2\right) \\ K_4 = \left(1 + x_m^2\right)^2 \end{cases} \tag{13}$$

Then, the coefficients of (11) can be calculated directly after mathematical matching, those are

$$\begin{cases} \boldsymbol{c_0} = \dfrac{x_{c1}^2 x_{c2}^2 + x_m^4 + x_{c1}^2 x_m^4 + x_{c2}^2 x_m^4}{2} - x_{c1}^2 x_{c2}^2 x_m^2 \left(1 + x_m^2\right) \\ \boldsymbol{c_2} = \dfrac{x_{c1}^2 x_{c2}^2 - x_{c1}^2 - x_{c2}^2}{2} + x_m^2 \left(x_m^2 - 1 - 2x_{c1}^2 - 2x_{c2}^2\right) \\ \boldsymbol{d_0} = \dfrac{\left(1 + x_{c1}^2 + x_{c2}^2\right) x_m^4 - x_{c1}^2 x_{c2}^2 \left(1 + 2x_m^2\right)}{2\varepsilon} \\ \boldsymbol{d_6} = \dfrac{x_{c1}^2 + x_{c2}^2 - 2x_m^2}{\varepsilon} \end{cases} \tag{14}$$

Finally, the admittances can be obtained by solving the equations in (2) with (15)

$$\begin{cases} a_0 = c_0 \\ a_2 = c_2 \\ b_0 = d_0 \\ b_6 = d_6 \end{cases} \tag{15}$$

The synthesis procedure is summarized in Fig.3. When the three in-band specifications (θ_{c1}, θ_{c2}, and ε) are fixed, the solution set (y_1, y_2, y_c and y_s) will change as θ_m changes.

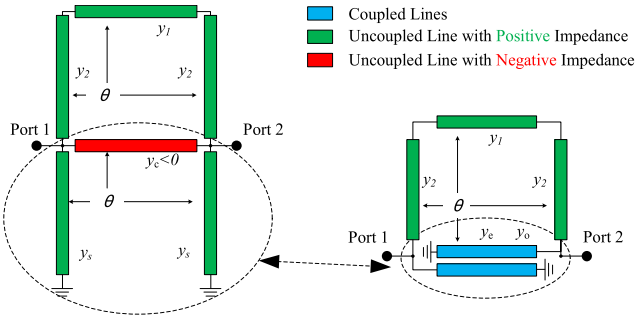

FIGURE 4. Realization of stub loaded ring with negative admittance.

Comparing with the other synthetic designs such as [8], [9], and [11] with one fixed response type, this unique property offers an extra tuning freedom, and also, provides multiple and tunable responses depending on θ_m. In [18], we have discussed such an operation on single-band delay already. In the following, we will show the response diversity of this structure by applying this mechanism.

Let us categorize the solution sets according to the ($\pm$) signs of y_c and y_1, which depend strongly on θ_m . The other two admittances (y_2 and y_s) are always positive in every case.

A. CASE #1: $y_c > 0$ & $y_1 > 0$

When y_c is positive, the bottom line can be implemented directly as shown in Fig.1a. A BPF with an embedded equalizer can be obtained after optimization [18]. The delay response can be tuned to be equiripple to achieve the minimal variation within the passband. The only drawback is that the out-band rejection will be affected more or less. With the improved synthesis procedure here, a new BPF with dual-passband can be implemented in this case, too.

B. CASE #2: $y_c = 0$ & $y_1 > 0$

After unfolding, it has exactly the same structure as an MMR filter [9], which has a fourth-order Chebyshev response in magnitude. In this case, θ_m is not free, and can be determined from $\theta_{c1}(\theta_{c2} = 90°)$, according to [9].

C. CASE #3: $y_c < 0$ & $y_1 > 0$

In the third case, the line (y_c) has a negative admittance that cannot be implemented directly, as shown in Fig.1c. Fortunately, the negative admittance line (y_c), together with two shunt stubs (y_s), can be equivalent to a shorted-coupled-line section [19] by using (16). It is interesting that after transformation, the structure is similar to two signal interference filters [16], [17], as shown in Fig.4. However, the original design methodologies in [16] and [17] are not capable of obtaining equiripple response directly. Here, the exact synthesis procedure about this structure is given for the first time. In addition, this structure is suitable for building dual-band BPF, too.

$$\begin{cases} y_o = y_s \\ y_e = 2y_c + y_s \end{cases} \qquad y_s > 0,\ y_c < 0 \tag{16}$$

TABLE 1. Parameters of comparison set (single passband).

Parameter	θ_{c1}	ε	θ_m	$\|S_{11}\|$ Ripple	y_1	y_2	y_c	y_s	y_e	y_o	*Response type*	*Remarks*
Unit	Degree	N/A	Degree	dB	N/A				N/A			
Case A	60.0	0.1005	70.3	-20.0	0.1871	0.4987	0.2239	1.1758	N/A		Equiripple Delay	Stub Loaded Ring [18]
Case B	60.0	0.1005	68.3	-20.0	0.2617	0.5379	0.0000	1.4225	N/A		Chebyshev	Stub Loaded MMR [9]
Case C	60.0	0.1005	67.8	-20.0	0.3195	0.5334	-0.2150	1.6920	1.2620	1.6920	Elliptic	Signal Interference Ring [16,17]
Case D	60.0	0.1807	67.0	-15.0	0.2823	0.5305	-0.2001	2.1388	1.7386	2.1388		
Case E	60.0	0.1005	67.8	-20.0	0.3439	0.4967	-0.3883	1.9339	1.1573	1.9339		
Remarks	Lower Cut-off Frequency	Ripple Factor	First Ripple Frequency		Normalized Admittance: Initial Strcuture				Normalized Admittance: Coupled line		θ_{c2}=90.0° FBW=66.7%	

D. CASE #4: $y_c > 0$ & $y_1 = 0$

In this case, the top line (y_1) is disconnected/isolated from other elements, as shown in Fig.1d. It is a well-known two staged BPF topology implemented by commensurate line [12], [13]. Considering the periodic response of commensurate line circuits, it also can be treated as a dual-band BPF.

E. CASE #5 $y_c = 0$ & $y_1 = 0$

When both the top and bottom lines are with zero admittance, Port 1 and Port 2 are totally isolated from each other, thus no transmission can be observed through the network.

F. CASE #6 $y_c < 0$ & $y_1 = 0$

In this case, a dual-band BPF can be obtained. After applying (16), it becomes a classic topology with two coupled resonators. Moreover, it can be categorized into *Case #4* with an external phase inverter, as proven in the *Appendix*.

G. CASE #7: $y_1 < 0$

Differing from *Case #3*, the negative admittance (y_1) here cannot be transformed into a realizable structure by using (16), because there is no stub loaded beside the top line (y_1).

Now, we have six Cases (#1-#6) that can be implemented in practical, within which only the first four (#1-#4) have bandpass responses. Each of them has a corresponding structure that has been reported before [9], [12], [13], [15], [16]. Based on the same synthesis procedure introduced above, one can find out the exact admittances easily. Comparing with the related synthesis methods such as [9] and [16], the proposed algorithm is advanced in supporting more structures, dual-band operation and precise equiripple response.

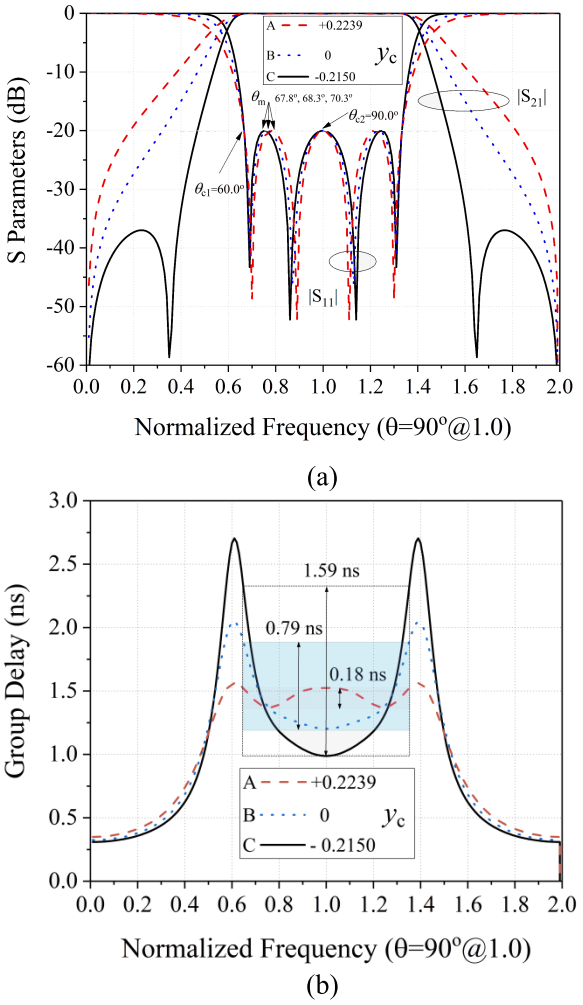

FIGURE 5. Single band frequency responses (different type) of stub loaded ring filter with same in-band specifications ($\theta_{c1} = 60.0°$, $\theta_{c2} = 90.0°$ and $\varepsilon = 0.1005$). (a) Magnitude. (b) Group Delay.

III. DISCUSSION ON DIVERSITY IN RESPONSE

In Part II, we have shown that for given in-band specifications (θ_{c1}, θ_{c2}, and ε), the solution sets with different θ_m will lead to different structures (#1-#4). Although two (#1 and #2) of the four have been described already in [9] and [18] for single-band operation, here, we would like to give a detailed, comparative discussion on their responses associated with that of Case #3 and #4 for both single- and dual- band operations.

A. SINGLE-BAND RESPONSE

In this section, the discussed filters have a single passband of 66.7% (2/3)*FBW* and a $|S_{11}|$ ripple of -20 dB ($\theta_{c1} = 60.0°$, $\theta_{c2} = 90.0°$, and $\varepsilon = 0.1005$). Fig.5 depicts the frequency responses of a comparison filter set. The related parameters are given in Table 1 as *Case A*, *B*, and *C*. Within the passband, it can be seen that all the three BPFs have equiripple response in magnitude, the only difference is the slight variation of θ_m. However, the responses are quite different in the stopband.

TABLE 2. Parameters of comparison set (dual passband).

Parameter	θ_{c1}	θ_m	θ_{c2}	*FBW*	ε	$\|S_{11}\|$ Ripple	y_1	y_2	y_c	y_s	y_e	y_o	$\|S_{21}\|$		*Topology*
Unit	Degree			%	N/A	dB	N/A				N/A		dB		
Case DA1	40.0	44.50	50.0	22.2	0.1005	-20.0	1.0996	2.4367	-0.4468	1.7249	0.8313	1.7249	-∞	-9.8	Signal Interference Ring [16,17]
Case DA2	40.0	45.00	50.0				0.2410	2.1381	0.3843	1.3859	N/A			-19.0	Stub Loaded Ring [18]
Case DA3	40.0	45.22	50.0				0	1.8984	0.7923	1.2788	N/A			-∞	Cascading Stub&Line [12,19]
Case DB1	58.0	59.80	62.0	6.7	0.1807	-15.0	0.7115	3.6820	-1.1248	10.4888	8.2392	10.4888		-20.1	Signal Interference Ring [16,17]
Case DB2	58.0	59.96	62.0				0.2312	3.5479	0.2149	9.5605	N/A			-24.1	Stub Loaded Ring [18]
Case DB3	58.0	60.06	62.0				0	3.3219	1.0390	9.0220	N/A			-∞	Cascading Stub&Line [12,13]
Remarks	Lower Cut-off Frequency	Ripple Frequency	Upper Cut-off Frequency		Ripple Factor	Both the passbands	Initial Strcuture				Coupled line		0°	90.0°	
	In First Passband (θ<90.0°)						Normalized Admittance								

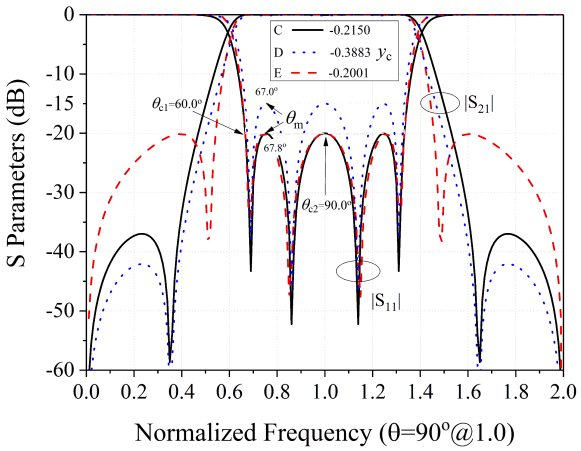

FIGURE 6. Single band frequency responses of stub loaded ring filter (*Case #3*) with transmission zeroes ($\theta_{c1} = 60.0°$ and $\theta_{c2} = 90.0°$).

A significant improvement on rejection can be observed in Case $C(y_c < 0)$ from Fig.5a, due to the extra two transmission zeroes which can be also found in the signal interference filters [16], [17]. An explanation on the transmission zeroes is that $Q(x^2)$ in (6) has two finite real roots beside the passband when $y_c < 0$. From Fig.5b, it can be seen that the delay variation of *Case A* is the minimal (0.18ns), whereas that of *Case C* is the maximal (1.59ns). One can now conclude that the better (worse) rejection in stopband, the worse (better) group delay in passband. It validates the compromise in filter design with limited circuit elements.

Another detailed comparison is made as a supplement focusing on *Case #3*, which has balanced magnitude response in both passband and stopband. From Fig.6, it can be observed that the ripple factor (ε) has no impact on the transmission zeroes. However, a better in-band matching leads directly to worse out-band rejections, e.g., selectivity and attenuation ripple in stopband, after comparing *Case C* with *D*. On the other hand, if the ripple factor (ε) and cut-off frequency (θ_c) are fixed (*Case C* and *E*), the selectivity and the attenuation ripple in stopband will restrict mutually according to the simulated results.

B. DUAL-BAND RESPONSE

Besides the single-band operation, the stub-loaded ring topology also supports dual-band when θ_{c2} is not locked at 90.0°. On the other hand, one can treat the dual-band response as a special case that the second ripple (A_0 in Fig.2) at $\theta = 90°$ of the single-band BPF, rises up from the other ripples at θ_m and θ'_m. Thus the continuous passband will be split into two discrete bands with a center notch, which is a traditional approach for dual-band BPF realization [12]. The two passbands are symmetrical to $\theta = 90°$ [12], [13], and have same bandwidth. We have designed six sample BPFs with dual passbands listed in Table 2. They are categorized into two sets according to center frequency and FBW.

Fig.7a shows the simulated responses of the first set BPFs, which are designed based on the specifications of ($\theta_{c1} = 40.0°$, $\theta_{c2} = 50.0°$, and $\varepsilon = 0.1005$), namely, ($FBW = 22.2\%$, $|S_{11}|$ ripple $= -20$ dB and center frequency of 45°). Due to the symmetry, one can find that the frequency ratio of the two bands is 3:1 exactly, which is the most common case in commensurate BPF design. It is clear that all the three filters exhibit the desired in-band response successfully. The modulation from θ_m, on the out-band rejection, is still effective as in the single-band case. When θ_m moves towards lower frequency, the rejection in the low band is strengthened (for the first passband), whereas the rejection in the high band is weakened. In the case of smaller θ_m, the bottom line (y_c) may have negative admittance (*Case DA*1), which means this BPF has the same topology with that in *Case* #3, and surely can be realized in practical with the same physical structure. Moreover, when θ_m moves towards the other direction, especially at a particular frequency (45.22°), the admittance of the top line (y_1) will equal to zero (*Case DA*3). The ring structure is now changed to a cascading structure with linear configuration [12], [13], which means there is only one signal passage without interference from multiple passages. The advantage is that the attenuation at $\theta = 90.0°$ is infinite, which enhances the rejection level between the two passbands tremendously.

Without loss of generality, another set BPFs (*Case DB*$1-3$ in Table 2) are given for comparison. From Fig.7b, one can find the in-band $|S_{11}|$ ripple is -15 dB, and frequency ratio of two bands is about 1.9. Similar responses can be observed comparing with *Case DA*. The main difference is that there exists a transmission zero at the lower rejection band (of the first passband) when y_c is negative. This property is useful for improving the stopband response at specific frequency point. In fact, in *Case DA*, the transmission zero will appear when θ_m is smaller enough, however, the rejection in the other side

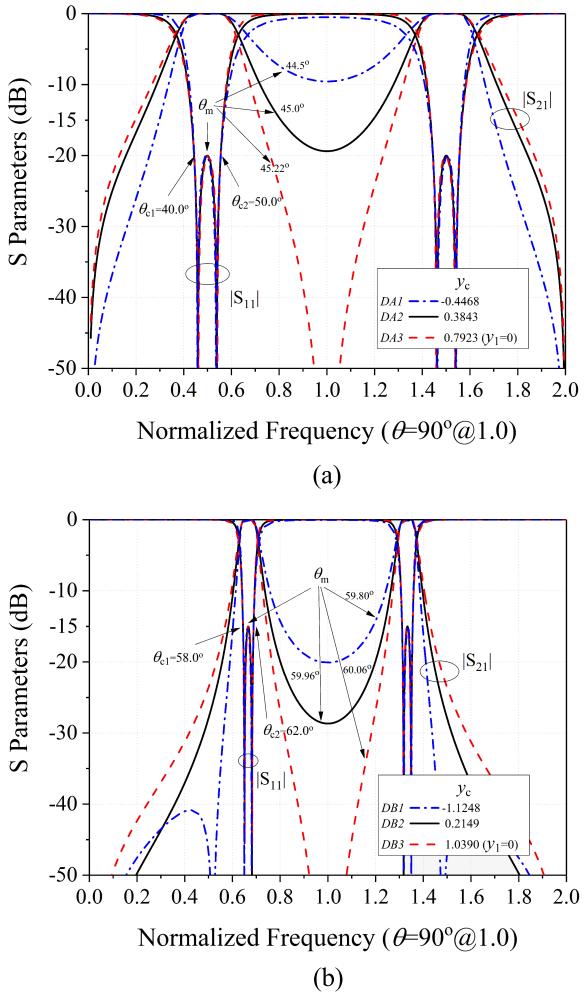

FIGURE 7. Dual-band frequency responses of stub loaded ring filters. (a) *Case DA* ($\theta_{c1} = 40.0°$, $\theta_{c2} = 50.0°$ and $\varepsilon = 0.1005$). (b) *Case DB* ($\theta_{c1} = 58.0°$, $\theta_{c2} = 62.0°$ and $\varepsilon = 0.1807$).

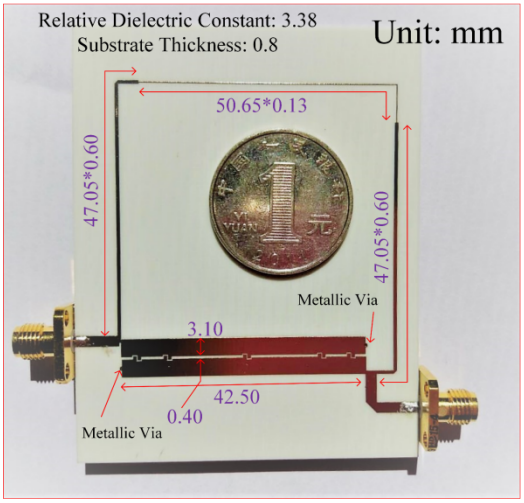

FIGURE 8. Photograph of fabricated filter (Table 1: *Case C*).

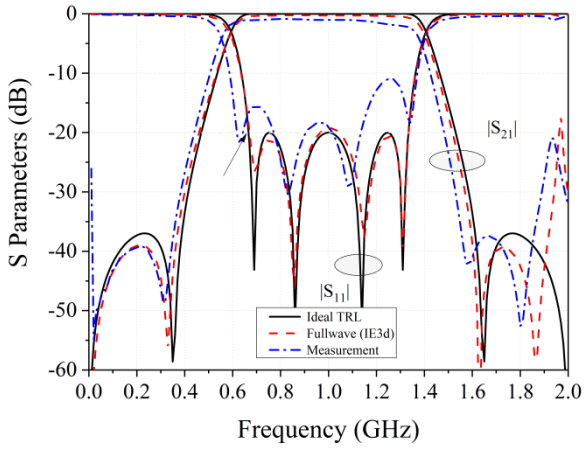

FIGURE 9. Ideal, fullwave, and measured magnitude response of *Case C* in Table 1.

(between the two bands) will be affected to an unacceptable level as the trend shown in Fig.7a. Since the main objective of this paper is the response diversity of the ring topology, more detailed discussions on the dual-band response of this topology will not be demonstrated further.

In addition, the proposed synthesis approach may be capable of other commensurate line filters, e.g., bandstop and/or lowpass filters, if the topology itself supports equiripple magnitude response. The key is that the sum of the number of the unknowns (line admittances) and the number of the relationship equations (of the coefficients of the transfer function, as in (12) or (2)) must be equal to the total number of the coefficients, as in (1) or (2).

IV. EXPERIMENTAL VERIFICATION

For practical verification, we choose *Case C* as a filter sample for fabrication. Before circuit simulation, the negative admittance line with two short-ended stubs together, have been transformed into a coupled line section, according to (16). A commercial Software, *IE3d*, is adopted for fullwave simulations. In the microstrip layout, a simple, efficient and powerful technique [20] is applied for compensating the velocity difference between the odd and the even modes of the coupled line section, as can be seen in Fig.4. The actual filter is constructed on a microstrip substrate (*Rogers 4003*) with height of 0.8 mm and relative dielectric constant of 3.38. The fabricated sample is shown in Fig.8, marked with detailed dimensions. Two SMA connectors are used for *S*-parameter test, through a VNA (*R&S ZVA67*). The measured results, together with the ideal and the fullwave simulated data, are shown in Fig.9. In all cases, two transmission zeroes nearby the passband can be observed clearly. Since the equiripple response observed in measurement is not perfect, here the 3-dB FBW will be used for comparison. The measured 3-dB FBW is 86.6%, centered at 0.97GHz, whereas the 3-dB FBW of the ideal case is 82.0%. Within the passband, the minimal measured insertion loss is about 0.88 dB at 0.81 GHz, including the loss from SMA connectors. The difference between the measured and the simulated results is mainly caused by the uncertainty of the substrate's permittivity, because the

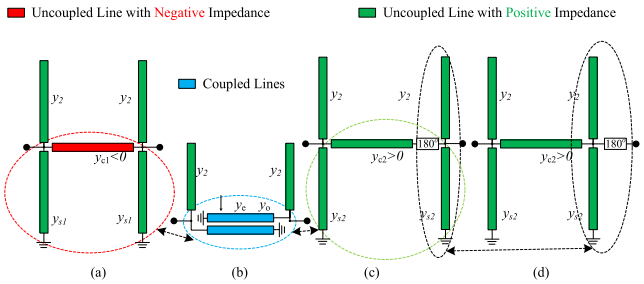

FIGURE 10. Equivalences between stub loaded line circuits. (a) Initial topology of *Case* #6 (Negative line). (b) Coupled line form of *Case* #6. (c) Equivalent circuit with all positive lines and internal phase inverter. (d) Equivalent circuit with all positive lines with external phase inverter (*Case* #4 with Phase inverter).

measured response is moved towards the lower frequency in general, comparing with the simulated response. The non-equiripple response in measured $|S_{11}|$is mainly due to the manufacture tolerance. The main objective of this experiment is to verify the effectiveness of this topology and the synthesis procedure, which is already achieved by the fullwave simulation, that agrees perfectly with the ideal transmission line models, as illustrated in Fig.9.

V. CONCLUSION

It is found that a particular topology of stub loaded commensurate line ring is shared by four different filters with different responses (after circuit transformation). As a result, a generalized synthesis method is developed. When the in-band specifications are fixed, the frequency response in both magnitude and delay can be tuned by varying an extra parameter which indicates the first reflection ripple within the passband. The location of the first ripple dominates the response type, e.g., equal ripple in delay, Chebyshev in magnitude, and elliptic in magnitude. It also leads to different solutions which may have zero or negative line admittance, as well as different structures in practical implementation. The diversity in response may be useful for reconfigurable filter design. In future work, we will apply this synthesis method to other filter topologies, or higher order filters with improved performance.

APPENDIX

In Part II, we have stated that *Case #4* ($y_c > 0$) and *Case #6* ($y_c < 0$) share the same topology. As shown in Fig.10a, the initial structure in Case #6 can be transformed into its coupled line form (Fig.10b) using (16). After applying a well-known formula (17) from [3],

$$\begin{cases} y_o = 2y_{c2} + y_{s2} \\ y_e = y_{s2} \end{cases} \qquad y_s > 0,\ y_c > 0 \qquad (17)$$

the first equivalent circuit of *Case #6* without negative element can be obtained as shown in Fig10c. Note that there is an ideal phase inverter placed between the connecting line (y_{c2}) and stubs (y_2 and y_{s2}). Because $y_1 = 0$, namely there is only one signal passage between the input/output ports, the location of the phase inverter and the shunt stubs (y_2 and y_{s2}) can be swapped directly without any impedance transformation, as given in Fig.10d. Comparing Fig.10d with Fig.1d, one can find that the two circuits are almost the same, except an ideal phase shifter which has no impact on magnitude and delay responses at all. Therefore, we have proved that *Case #6* is the same as *Case #4* in magnitude and delay responses.

However, the equivalence between *Case #4* and *#6* is not applicable for Case #1 and #3 that also have similar topologies. In the latter two cases, since $y_1 > 0$, the phase inverter cannot be moved out from the ring, and cannot be dismissed after applying (16) and (17).

ACKNOWLEDGEMENT

The authors would like to thank Saili Chen and Wenyan Li a lot for data gathering and visualization. They would like to thank the reviewers and editors for their professional suggestions, which help us greatly in improving the quality of this manuscript.

REFERENCES

[1] L. Zhu, S. Sun, and W. Menzel, "Ultra-wideband (UWB) bandpass filters using multiple-mode resonator," *IEEE Microw. Wireless Compon. Lett.*, vol. 15, no. 11, pp. 796–798, Nov. 2005. doi: 10.1109/LMWC.2005.859011.

[2] R. J. Cameron, C. M. Kudsia, and R. Mansour, *Microwave Filters for Communication Systems: Fundamentals, Design and Applications*. New York, NY, USA: Wiley, 2007.

[3] J.-S. Hong and M. J. Lancaster, *Microstrip Filters for RF / Microwave Applications*. New York, NY, USA: Wiley, 2001.

[4] Z.-C. Hao and J.-S. Hong, "Ultrawideband filter technologies," *IEEE Microw. Mag.*, vol. 11, no. 4, pp. 56–68, Jun. 2010. doi: 10.1109/MMM.2010.936494.

[5] L. Zhu, S. Sun, and W. Menzel, "Ultra-wideband (UWB) bandpass filters using multiple-mode resonator," *IEEE Microw. Wireless Compon. Lett.*, vol. 15, no. 11, pp. 796–798, Nov. 2005. doi: 10.1109/LMWC.2005.859011.

[6] A. Kamma, R. Das, D. Bhatt, and J. Mukherjee, "Multi mode resonators based triple band notch UWB filter," *IEEE Microw. Wireless Compon. Lett.*, vol. 27, no. 2, pp. 120–122, Feb. 2017. doi: 10.1109/LMWC.2017.2649383.

[7] B. Yao, Y. Zhou, Q. Cao, and Y. Chen, "Compact UWB bandpass filter with improved upper-stopband performance," *IEEE Microw. Wireless Compon. Lett.*, vol. 19, no. 1, pp. 27–29, Jan. 2009. doi: 10.1109/LMWC.2008.2008558.

[8] R. Li, S. Sun, and L. Zhu, "Synthesis design of ultra-wideband bandpass filters with composite series and shunt stubs," *IEEE Trans. Microw. Theory Techn.*, vol. 57, no. 3, pp. 684–692, Mar. 2009. doi: 10.1109/TMTT.2009.2013312.

[9] R. Zhang and L. Zhu, "Synthesis design of a wideband bandpass filter with inductively coupled short-circuited multi-mode resonator," *IEEE Microw. Wireless Compon. Lett.*, vol. 22, no. 10, pp. 509–511, Oct. 2012. doi: 10.1109/LMWC.2012.2218096.

[10] G. L. Matthaei, L. Young, and E. M. T. Jones, *Microwave Filters, Impedance-Matching Networks, and Coupling Structures*. Dedham, MA, USA: Artech House, 1980.

[11] M. C. Horton and R. J. Wenzel, "General theory and design of optimum quarter-wave TEM filters," *IEEE Trans. Microw. Theory Techn.*, vol. 13, no. 3, pp. 316–327, May 1965. doi: 10.1109/TMTT.1965.1125996.

[12] A.-S. Liu, T.-Y. Huang, and R.-B. Wu, "A dual wideband filter design using frequency mapping and stepped-impedance resonators," *IEEE Trans. Microw. Theory Techn.*, vol. 56, no. 12, pp. 2921–2929, Dec. 2008. doi: 10.1109/TMTT.2008.2007357.

[13] R. Zhang, S. Luo, L. Zhu, and L. Yang, "Synthesis and design of miniaturized wideband bandpass filters with scaled transmission line for spurious-response suppression," *IEEE Trans. Microw. Theory Techn.*, vol. 65, no. 8, pp. 2878–2885, Aug. 2017. doi: 10.1109/TMTT.2017.2668411.

[14] X. Jin, X. Huang, D. Chen, and C. Cheng, "Compact wideband bandpass filter with equiripple response in both magnitude and delay," *Int. J. RF Microw. Comput.-Aided Eng.*, vol. 28, no. 6, Aug. 2018, Art. no. e21293. doi: 10.1002/mmce.21293.
[15] W. Feng, W. Che, and Q. Xue, "Transversal signal interaction: Overview of high-performance wideband bandpass filters," *IEEE Microw. Mag.*, vol. 15, no. 2, pp. 84–96, Mar./Apr. 2014. doi: 10.1109/MMM.2013.2296216.
[16] M. Á. Sanchez-Soriano, E. Bronchalo, and G. Torregrosa-Penalva, "Compact UWB bandpass filter based on signal interference techniques," *IEEE Microw. Wireless Compon. Lett.*, vol. 19, no. 11, pp. 692–694, Nov. 2009. doi: 10.1109/LMWC.2009.2032001.
[17] W. Feng and W. Che, "Novel ultra-wideband bandpass filter using shorted coupled lines and transversal transmission line," *IEEE Microw. Wireless Compon. Lett.*, vol. 20, no. 10, pp. 548–550, Oct. 2010. doi: 10.1109/LMWC.2010.2055840.
[18] X. Jin, X. Huang, D. Chen, and C. Cheng, "Stub-loaded square loop bandpass filter with equiripple response in both delay and magnitude," *Int. J. RF Microw. Comput.-Aided Eng.*, vol. 28, no. 8, Oct. 2018, Art. no. e21297. doi: 10.1002/mmce.21297.
[19] R. Zhang, S. Luo, and L. Zhu, "A new synthesis and design method for wideband bandpass filters with generalized unit elements," *IEEE Trans. On Microw. Theory And Techn.*, vol. 65, no. 3, pp. 815–823, Mar. 2017. doi: 10.1109/TMTT.2016.2636825.
[20] S. Gruszczynski and K. Wincza, "Generalized methods for the design of quasi-ideal symmetric and asymmetric coupled-line sections and directional couplers," *IEEE Trans. Microw. Theory Techn.*, vol. 59, no. 7, pp. 1709–1718, Jul. 2011. doi: 10.1109/TMTT.2011.2138155.

XIUHUA JIN was born in Jiangsu, China, in 1983. She received the Ph.D. degree in electronic science and engineering from the Nanjing University of Posts and Telecommunications, China, in 2014, where she is currently a Lecturer. Her current research interests include microwave passive circuit and electromagnetics.

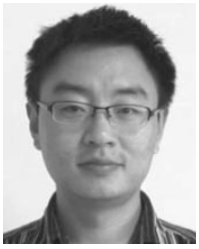

XIAODONG HUANG was born in Shanxi, China, in 1980. He received the Ph.D. degree in electronic science and engineering from the Nanjing University of Posts and Telecommunications (NUPT), China, in 2011. From 2008 to 2009, he was a Research Associate with Nanyang Technological University, Singapore. He is currently an Associate Professor with NUPT. His current research interests include wideband antenna and microwave passive circuit.

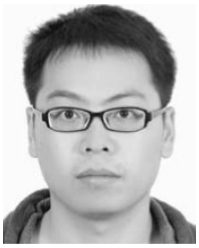

DONG CHEN received the Ph.D. degree in electronic engineering from the Nanjing University of Posts and Telecommunications, Nanjing, China, in 2010, where he has been an Assistant Professor of electromagnetic fields, since 2014. His current research activities are mainly concerned with the design of the microwave and RF antenna, transceiver, and power amplifier.

CHONGHU CHENG (M'01) received the B.S., M.S., and Ph.D. degrees from Southeast University, Nanjing, China, in 1983, 1986, and 1993, respectively, all in electronic science and engineering. From 1994 to 1996, he was a Postdoctoral Researcher with the Department of Information Electronics, Zhejiang University, China. From 1996 to 1999, he served as a Lecturer with Hainan University, China. From 1999 to 2001, he was a Research Fellow with the National Institute of Information and Communications Technology, Japan. He joined the College of Telecommunications and Information Engineering, Nanjing University of Posts and Telecommunications, as an Associate Professor, in 2011, and became a Full Professor, in 2006. He has authored or co-authored more than 100 technical publications. His research interests include computational electromagnetics, small antennas, and microwave passive circuits. He is a member of the China Institute of Electronics, Antenna Society. He served as a Reviewer for several international journals, including the IEEE Microwave and Wireless Components Letters and *Electronics Letters*.